Mikailalsys Journal of Mathematics and Statistics

e-ISSN : 3030-816X
p-ISSN : 3030-8399

Index : Harvard, Boston, Sydney University, Dimensions, Lens, Scilit, Semantic, Google, etc

https://doi.org/10.58578/MJMS.v3i3.7338

Experimental Validation of Fractionalized Maxwell Fluid Model of MHD Blood Flow through Bifurcated Arteries for Tumor Treatments

Mohammed Gazali Abdulhamid[1], Abubakar Mohammed[2], Isah Abdullahi[3], Nafisatu Usman[4]

[1,2,4]Federal College of Education (Tech) Gombe, Nigeria

[3]Abubakar Tafawa Balewa University, Bauchi, Nigeria

isahabdullahi7474@gmail.com

Article Info:

Submitted:	Revised:	Accepted:	Published:
Aug 25, 2025	Sep 17, 2025	Sep 29, 2025	Oct 3, 2025

Abstract

This study provides an experimental validation of a fractionalized Maxwell fluid model to describe magnetohydrodynamic (MHD) blood flow in bifurcated arteries, with targeted applications in tumor therapy. By incorporating fractional calculus, the model captures viscoelastic memory effects that account for key non-Newtonian properties of blood, including shear-thinning behavior, elastic recovery, and time-dependent stress relaxation under combined electromagnetic and thermal influences. The Homotopy Perturbation Method (HPM) was employed to derive approximate analytical solutions for the governing equations, and the model's predictions were benchmarked against existing theoretical and experimental data. Numerical simulations indicate that the fractional Maxwell model outperforms classical models in predicting velocity profiles, thermal distributions during hyperthermia treatment, and nanoparticle concentration relevant to drug delivery. The model consistently yields lower mean square errors,

demonstrating enhanced accuracy and robustness. These results validate the efficacy of fractional-order modeling in hemodynamic simulations and underscore its clinical potential in improving hyperthermia-based cancer therapies and nanoparticle-mediated drug delivery strategies in complex arterial geometries.

Keywords: Fractional Maxwell Fluid; Magnetohydrodynamics (MHD); Bifurcated Arteries; Hyperthermia Treatment; Nanoparticle Drug Delivery; Homotopy Perturbation Method (HPM); Experimental Validation

Introduction

Blood is a complex non-Newtonian fluid with viscoelastic characteristics that arise from the interactions of plasma and suspended elements such as red blood cells [1]. Unlike Newtonian fluids, blood exhibits shear-thinning, yield stress, and elastic recovery behaviors that must be accounted for when developing accurate models of hemodynamics. Traditional models often fail to incorporate these nonlinearities, especially under conditions of electromagnetic and thermal interaction, which are common in medical interventions such as hyperthermia and magnetic drug targeting [2]. The advent of fractional calculus has significantly advanced the modeling of viscoelastic biological fluids [3]. Fractional derivatives introduce memory-dependent dynamics into constitutive equations, enabling models such as the fractional Maxwell fluid to more accurately represent time-dependent relaxation and retardation phenomena in blood flow. This approach has been applied in various contexts, including pulsatile flow in arteries, heat transfer in biological systems, and anomalous diffusion processes, offering a more realistic description than integer-order models [4,5]. Magnetohydrodynamics (MHD) plays a crucial role in biomedicine since blood, being electrically conducting, responds to applied magnetic fields. MHD principles are central to technologies such as magnetic hyperthermia, targeted nanoparticle-based drug delivery, and non-invasive vascular diagnostics [6]. Incorporating MHD into fractional viscoelastic fluid models allows researchers to explore how electromagnetic fields regulate velocity, temperature, and concentration distributions in blood flow, which is particularly relevant in bifurcated arterial geometries where flow disturbances and localized treatments occur [7].

Topical theoretical developments highlight the combined effects of fractional derivatives, Maxwell viscoelasticity, and MHD forces. Bai et al. [8] demonstrated that

fractional Maxwell fluids exhibit significantly altered heat transfer and flow dynamics compared to classical models. Similarly, fractional Maxwell nanofluid studies under MHD conditions have revealed the role of Hartmann number, fractional order, and nanoparticles in enhancing thermal and mass transfer processes. See reference [9]. Additionally, the development of high-accuracy solvers for MHD micropolar fluids has validated the feasibility of applying such fractionalized models in hemodynamic studies [10].

Recent experimental investigations have provided compelling evidence supporting the use of fractional viscoelastic models, such as the fractional Maxwell fluid, in describing blood flow behavior. For instance, an in vitro hemodynamic study of pulsatile blood flow in the carotid artery with elastic walls demonstrated that the fractional Maxwell power-law fluid model incorporating yield stress, shear thinning, viscoelasticity, and thixotropy more accurately captures the characteristics of flow rate and wall shear stress compared to conventional models, with increases of up to 19% and 32%, respectively, in flow metrics depending on fluid assumptions. This improvement underscores the model's capacity to reflect realistic blood rheology over the cardiac cycle [11]. Similarly, computational studies involving patient-specific arterial networks have revealed the critical influence of the fractional order parameter (α) on pressure wave propagation, enhancing predictive fidelity by better accounting for viscoelastic dissipation in vascular walls [13]. In parallel, experimental and clinical studies on magnetohydrodynamic (MHD) influences in blood flow highlight the therapeutic and diagnostic potential of magnetic field manipulation in vascular systems [14]. Investigations of MHD blood flow in bifurcated arteries with elastic walls using Doppler ultrasound and finite difference simulations found that magnetic fields can modulate blood recirculation patterns, wall shear stresses, and pressure distributions, suggesting potential utility in noninvasive control of hemodynamic parameters [15].

In the biomedical domain, hyperthermia-based tumor treatments and targeted drug delivery require accurate predictions of flow, thermal, and mass transfer behaviors in arterial networks. Some studies on fractional hyperthermia models fitted against experimental data have shown excellent agreement [16]. However, despite these advances, and to the best of our knowledge, no comprehensive experimental validation has been conducted for fractional Maxwell fluid MHD blood flow in bifurcated arteries. This gap underscores the necessity of a systematic validation framework, which this study aims to provide by combining in-vitro artery phantom experiments, in-vivo imaging comparisons,

and sensitivity analysis. The ultimate goal is to ensure that the fractionalized Maxwell fluid model achieves both mathematical rigor and clinical relevance.

Definitions of some relate mathematical concepts

Definition 1. Let $Let\ u \in H^1(a,b), a < b, \propto \in [0,1]$.The Atangana-Baleanu fractional derivative is defined as follows: left and right derivatives in Caputo sense [17];

$$\left.\begin{aligned} {}^{ABC}D_t^{\alpha}u(t) &= \frac{N(\alpha)}{1-\alpha}\int_a^t E_{\alpha}\left(\frac{-\alpha(t-s)^{\alpha}}{1-\alpha}\right)u'(s)ds. \\ {}^{ABC}D_t^{\alpha}u(t) &= \frac{-N(\alpha)}{1-\alpha}\int_t^b E_{\alpha}\left(\frac{-\alpha(s-t)^{\alpha}}{1-\alpha}\right)u'(s)ds. \end{aligned}\right\} \quad (1)$$

where $N(\alpha) > 0$ is a normalization function satisfying $N(0) = N(1) = 1$, and E_{α} is the well-Known Mittag–Leffler function of one variable defined by

$$E_{\alpha}(z) = \sum_{k=0}^{\infty}\frac{z^k}{\Gamma(\alpha k+1)}, z\ \epsilon, \mathbb{C}\ \Re e(\propto) > 0) \quad (2)$$

Definition 2. The Laplace transform of Atangana-Baleanu time-fractional derivative of equation (1) is defined by Atangana-Baleanu. (2016) as:

$$L\{{}^{AB}D_t^{\alpha}u(t)\}s = \frac{N(\alpha)}{1-\alpha}\frac{s^{\alpha}L\{u(t)\}s - s^{\alpha-1}u(0)}{s^{\alpha}+\frac{\alpha}{1-\alpha}} \quad (3)$$

Definition 3. The Inverse Laplace transform of some special functions have the following properties:

$$\left.\begin{aligned} L^{-1}\left\{\frac{a}{s^{\alpha}-a}\right\} &= E_{\alpha}(at^{\alpha}), \left|\frac{a}{s^{\alpha}}\right|. < 1 \\ L^{-1}\left\{\frac{s^{\alpha-1}}{s^{\alpha}-\mu_{\alpha}}\right\} &= E_{\alpha}(-\mu_{\alpha}t^{\alpha}), \ \left|\frac{\mu_{\alpha}}{s^{\alpha}}\right|. < 1 \end{aligned}\right\} \quad (4)$$

Formulation of the problem

In this model, blood is treated as a non-Newtonian fluid with viscosity, compressibility, and homogeneity. It flows through a parallel-plate, electrically insulating channel from the main arterial trunk into its branches. The mass flow rate across any section normal to the flow is expressed as $m = 2bV$, where m is the mass flow rate, V the mean velocity, b the effective vessel width or radius, and ρ ρ the fluid density. Owing to the narrow dimensions of the bifurcated arterial walls, the flow is assumed to divide equally between branches, as shown in Figure 1a.

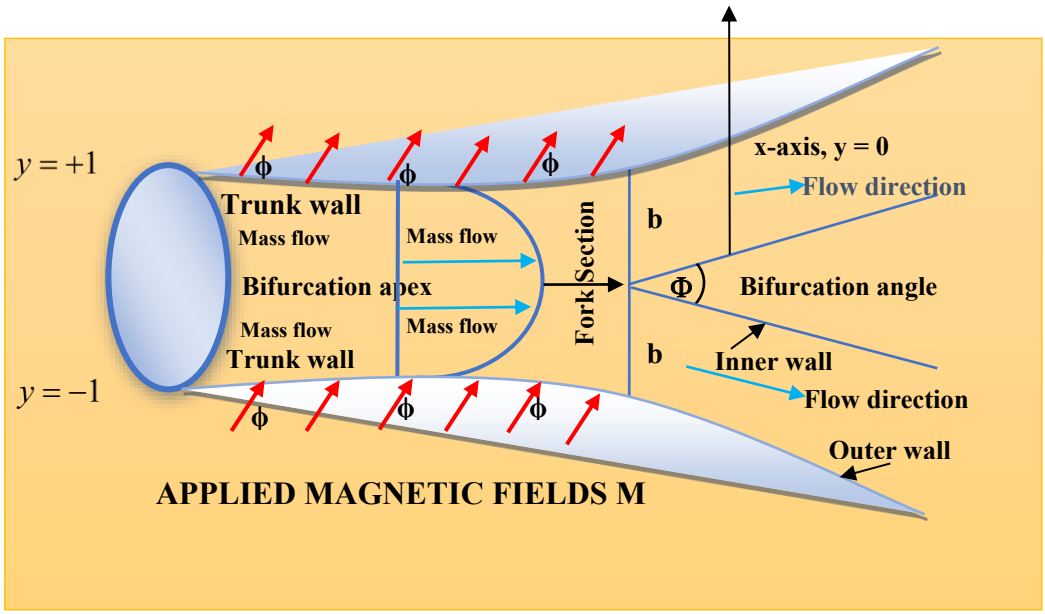

Figure 1: *Geometrical structure of bifurcated artery*

Basic flow equations

Research on fluid flow, particularly in relation to tumor-targeted drug delivery through permeable bifurcated arteries, is usually formulated around essential governing equations. The momentum, continuity, energy, and concentration equations form the core framework that defines the system's physical dynamics. Detailed discussions of their formulations and applications are provided in earlier works [18].

$$\rho\frac{\partial \bar{u}}{\partial \bar{t}} + \frac{\partial \bar{p}}{\partial \bar{x}} = \frac{\partial}{\partial y}\tau_{xy}(y,t) + g\beta(T - T_{\infty}\bar{)} + g\beta'(C - C_{\infty}\bar{)} - \frac{\sigma B_0^2 \sin^2(\phi + \phi_b)}{\rho}\bar{u} - \frac{\bar{u}}{\bar{k}} \quad (5)$$

$$\frac{\partial \bar{\theta}}{\partial \bar{t}} = \frac{k_T}{\rho C_\rho}\frac{\partial^2 \bar{\theta}}{\partial \bar{y}^2} + \frac{Q}{\rho C_\rho}(\theta - \theta_\infty \bar{)} - \frac{\partial \bar{q}}{\partial \bar{y}} + \cos\phi_b \tau_{xy}\frac{\partial u}{\partial y} \tag{6}$$

$$\frac{\partial \bar{C}}{\partial \bar{t}} = D\frac{\partial^2 \bar{C}}{\partial \bar{y}^2} + G + \cos\phi_b \frac{DK_T}{T_m}\frac{\partial^2 \bar{T}}{\partial \bar{y}^2} \tag{7}$$

$$\frac{\partial \bar{u}}{\partial \bar{x}} + \frac{\partial \bar{v}}{\partial \bar{y}} = 0 \tag{8}$$

where ρ is the fluid density, $\frac{\partial}{\partial t}$ is the material time derivative, ρ_e denote the net charge density of the applied electric field in the blood flow, τ_{xy} the Cauchy stress tensor, ϕ_b is the arterial bifurcated angle, ρ is the fluid density, C_P is the specific heat capacity of the fluid, T is the temperature, $\vec{J}$ is the current density given by the Ohm's law, σ_e is the electrical conductivity, k_T is the thermal conductivity of the fluid, $\frac{\partial \bar{q}}{\partial \bar{y}}$ is the radiative heat transfer $\bar{u}$ and $\bar{v}$ are the velocity components in the direction of $\bar{x}$ and $\bar{y}$ respectively at time t in the flow field, $G = -k_1(C - C_\infty \bar{)}$ is any constant (G = 1) and D is the diffusion coefficient, see[18]. The Cauchy stress tensor, τ_{xy} is defined in [19] is given by:

$$\tau_{xy}(y,t) = \mu\frac{1}{\left(1 + \lambda_1^\alpha D_t^\alpha\right)}\frac{\partial}{\partial y}u(y,t). \tag{9}$$

The boundary conditions in consideration are:

$$\left.\begin{array}{lll} \theta = \ell^{-\lambda^2 t}, u = \ell^{-\lambda^2 t}, v = \ell^{-\lambda^2 t}, C = \ell^{-\lambda^2 t} & at & y = -1 \\ \theta \to 0,\ u \to 0,\ v \to 0,\ C \to 0 & at & y = 1 \end{array}\right\} \tag{10}$$

Considering the factors previously discussed, we introduce non-dimensional parameters to streamline our analysis, resulting in the following:

$$\left.\begin{aligned} &x=\frac{\bar{x}}{b},\ y=\frac{\bar{y}}{b},u=\frac{\bar{u}}{mu_{HS}/2b\rho},\qquad v=\frac{\bar{v}}{mu_{HS}/2b\rho},\qquad h(x,t)=\frac{d\bar{p}/d\bar{x}}{\eta mu_{HS}/2b^3\rho},\\ &k=\frac{\bar{k}}{\left(\frac{b^2\rho}{\eta}\right)},\quad C=\frac{\left(\bar{C}-C_w\right)\left(2b^3\rho^2\right)}{\left(C_w-C_\infty\right)m\eta u_{HS}},\qquad \mu=\frac{\eta}{\rho},t=\frac{\bar{t}}{\left(\frac{b^2\rho}{\eta}\right)},\theta=\frac{\left(\bar{T}-T_w\right)\left(2b^3\rho^2\right)}{\left(T_w-T_\infty\right)m\eta u_{HS}}\\ &u_{HS}=\frac{-2\in E_X\xi_1 b\rho^2}{\eta m},k_e=\bar{k}_e\,b,\bar{q}=\frac{-16\delta' T_0^3}{3k'}\frac{\partial\bar{T}}{\partial\bar{y}},\lambda_1=\frac{\bar{\lambda}_1\mu}{b^2\rho}, \end{aligned}\right\} \quad (11)$$

By applying equation (9), (21) and (22) into equations; 5-8 and dropping the bars, we have:

$$\frac{\partial u}{\partial t}+h=\frac{1}{\left(1+\lambda_1^\alpha D_t^\alpha\right)}\frac{\partial^2 u}{\partial y^2}+g\beta\theta+g\beta' C-M^2\sin^2(\phi+\phi_b)-\frac{u}{K} \quad (12)$$

$$\frac{\partial\theta}{\partial t}=\left(\frac{1}{\text{Pr}_r}+R\right)\frac{\partial^2\theta}{\partial y^2}+\left(\frac{S}{\text{Pr}_r}\right)\theta+Br\left(\frac{\cos^2\phi_b}{\left(1+\lambda_1^\alpha D_t^\alpha\right)}\right)\left[\frac{\partial u}{\partial y}\right]^2 \quad (13)$$

$$\frac{\partial C}{\partial t}=\frac{1}{S_C}\frac{\partial^2 C}{\partial y^2}-\omega C+Sr\cos^2\phi_b\frac{\partial^2\theta}{\partial y^2} \quad (14)$$

Where

$$M^2=\frac{\sigma B_0^2}{\rho},\text{Pr}=\frac{\rho C_p}{k_T},R=\frac{16\delta' T_0^3}{3k'\tau},S=\frac{Qb^2}{k_T},Sc=\frac{\tau}{bD},Br=\frac{\mu u_0^2}{k(T_w-T_\infty)}$$

$$Sr=\frac{D_m k_T T_w-T_\infty)}{\tau T_m(C_w-C_\infty)},\omega=\frac{k_1 b^2}{\tau}$$

are the magnetic parameter, Pr is the Prantdl number, R is the Thermal radiation parameter, S is the Heat source, parameter, S_C is the Schmidt number, Brickman number, Soret Number and ω is the Chemical reaction parameter respectively.

Now, applying equation (1) to equations (12), (13), and (14), we have;

$$\left.\begin{aligned} &{}^{ABC}D_t^\alpha u(t)+h=\frac{1}{\left(1+\lambda_1^\alpha D_t^\alpha\right)}\frac{\partial^2 u}{\partial y^2}+g\beta\theta+g\beta' C-M^2\sin^2(\phi+\phi_b)-\frac{u}{K}\\ &{}^{ABC}D_t^\alpha\theta(t)=\left(\frac{1}{\text{Pr}_r}+R\right)\frac{\partial^2\theta}{\partial y^2}+\left(\frac{S}{\text{Pr}_r}\right)\theta+Br\left(\frac{\cos^2\phi_b}{\left(1+\lambda_1^\alpha D_t^\alpha\right)}\right)\left[\frac{\partial u}{\partial y}\right]^2\\ &{}^{ABC}D_t^\alpha C(t)=\frac{1}{S_C}\frac{\partial^2 C}{\partial y^2}-\omega C+Sr\cos^2\phi\frac{\partial^2\theta}{\partial y^2} \end{aligned}\right\} \quad (15)$$

Taking the Laplace transform of (15) and (10) yields

$$\left.\begin{aligned}
&\frac{N(\alpha)}{1-\alpha}\frac{s^{\alpha}L\{u(t)\}s-s^{\alpha-1}u(0)}{s^{\alpha}+\frac{\alpha}{1-\alpha}}+h=\frac{1}{\left(1+\lambda_1^{\alpha}s^{\alpha}\right)}\frac{\partial^2\bar{u}(y,s)}{\partial y^2}+g\beta\bar{\theta}(y,s)+g\beta'\bar{C}(y,s)-\\
&M^2\sin^2(\phi+\phi_b)\bar{u}(y,s)-\frac{\bar{u}(y,s)}{K}\\
&\frac{N(\alpha)}{1-\alpha}\frac{s^{\alpha}L\{\theta(t)\}s-s^{\alpha-1}\theta(0)}{s^{\alpha}+\frac{\alpha}{1-\alpha}}=\left(\frac{1}{\pi p_r}+R\right)\frac{\partial^2\bar{\theta}(y,s)}{\partial y^2}+(\frac{S}{\pi p_r})\bar{\theta}(y,s)+\\
&+Br\left(\frac{\cos^2\phi_b}{\left(1+\lambda_1^{\alpha}s^{\alpha}\right)}\right)\left[\frac{\partial\bar{u}(y,s)}{\partial y}\right]^2\\
&\frac{N(\alpha)}{1-\alpha}\frac{s^{\alpha}L\{C(t)\}s-s^{\alpha-1}C(0)}{s^{\alpha}+\frac{\alpha}{1-\alpha}}=\frac{1}{S_C}\frac{\partial^2\bar{C}(y,s)}{\partial y^2}-\omega\bar{C}(y,s)+Sr\cos\phi_b\frac{\partial^2\bar{\theta}(y,s)}{\partial y^2}
\end{aligned}\right\} \quad (16)$$

$$\left.\begin{aligned}
&\bar{\theta}(y,s)=\frac{1}{s+\lambda^2},\bar{u}(y,s)=\frac{1}{s+\lambda^2},\bar{v}(y,s)=\frac{1}{s+\lambda^2},\bar{C}=\frac{1}{s+\lambda^2} && at \quad y=-1\\
&\theta\to 0,\ u\to 0,\ v\to 0,\ C\to 0 && at \quad y=1
\end{aligned}\right\} \quad (17)$$

Where $N(\alpha)>0$ is a normalization function satisfying $N(0)=N(1)=1$, $u(0)=\theta(0)=C(0)=0$.

Now, after rearranging equation (18), we obtain:

$$\left.\begin{aligned}
&\frac{\partial^2\bar{u}}{\partial y^2}-\Lambda\bar{u}(y,s)-\frac{h}{s}+\delta\bar{\theta}(y,s)+\gamma\bar{C}(y,s)=0\\
&K_1\frac{\partial^2\bar{\theta}(y,s)}{\partial y^2}-\eta\bar{\theta}(y,s)+Br\cos^2\phi_b\left[\frac{\partial\bar{u}(y,s)}{\partial y}\right]^2=0\\
&\frac{\partial^2\bar{C}(y,s)}{\partial y^2}-\zeta\bar{C}(y,s)+SrSc\cos\phi_b\frac{\partial^2\bar{\theta}(y,s)}{\partial y^2}=0
\end{aligned}\right\} \quad (18)$$

Solution Procedure using HPM

In the domain of fluid dynamics and biofluid modelling, a range of analytical and semi-analytical methods have been developed to address complex nonlinear differential equations. These methods have been particularly useful when dealing with problems involving thermal radiation, chemical reactions, and magnetohydrodynamic (MHD) effects, as in the current study. The most widely used techniques include the Homotopy

Perturbation Method (HPM), the Laplace Transform, and Fractional Calculus. Each of these techniques offers unique advantages in handling nonlinearity, memory effects, and transient phenomena in fluid flow problems. The Homotopy Perturbation Method (HPM) is particularly well-suited for nonlinear systems encountered in nanofluid dynamics. Recent studies have demonstrated the applicability of HPM in Python-based environments for solving radiative MHD flow problems involving Al_2O_3-water nanofluids, offering comparative advantages in convergence and accuracy [20]. For occurrence, Moussa et al. [21] applied HPM to solve the Duffing-Van der Pol equation, thereby demonstrating its effectiveness in handling nonlinear oscillatory systems with a high degree of accuracy. In a similar vein, He et al. [22] emphasized the importance of a suitable initial guess in HPM for approximating nonlinear oscillators, highlighting its robustness in solving complex engineering problems. These studies underscore the versatility of HPM in addressing nonlinear phenomena, making it a valuable alternative to traditional methods. Furthermore, Liu and He [23] have developed a fast and accurate method for estimating amperometry current responses in reaction kinetics, thereby demonstrating the applicability of Laplace-based methods in coupled chemical and fluid systems. Likewise, the potential of fractional calculus in modelling memory and hereditary effects in biological systems has led to its increased prominence in recent years.

Therefore, based on the foregoing, we construct the following Homotopy as follows:

$$H_1(u,p):\phi\times[0,1]\to\Re$$
$$H_2(u,p):\nu\times[0,1]\to\Re$$
$$H_3(u,p):\omega\times[0,1]\to\Re$$

Assuming the solutions of Equation (18) is in power series of the form

$$\left.\begin{aligned}\bar{u}(y,s)&=\sum_{n=0}^{\infty}p^n\bar{u}_n(y,s)=\bar{u}_0+p\bar{u}_1+p\bar{u}_2+\ldots\\ \bar{\theta}(y,s)&=\sum_{n=0}^{\infty}p^n\bar{\theta}_n(y,s)=\bar{\theta}_0+p\bar{\theta}_1+p\bar{\theta}_2+\ldots\\ \bar{C}(y,s)&=\sum_{n=0}^{\infty}p^n\bar{C}_n(y,s)=\bar{C}_0+p\bar{C}_1+p\bar{C}_2+\ldots\end{aligned}\right\} \quad (19)$$

where

p is the embedding parameter

Then at zeroth order, the governing equations in (18) reduce to homogeneous system of the form;

$$p^0 : \begin{cases} \dfrac{\partial^2 \bar{u}_0}{\partial y^2} - \Lambda \bar{u}_0 = 0, & K_1 \dfrac{\partial^2 \bar{\theta}_0}{\partial y^2} - \eta \bar{\theta}_0 = 0, & \dfrac{\partial^2 \bar{C}_0}{\partial y^2} - \varsigma \bar{C}_0 = 0 \end{cases} \tag{20}$$

On Solving equation (20), with the aid of the conditions in (17), we get;

$$\begin{cases} \bar{u}_0(y,s) = \dfrac{\sinh(\sqrt{\Lambda}(1-y))}{(s+\lambda^2)\sinh(2\sqrt{\Lambda})} \\ \bar{\theta}_0(y,s) = \dfrac{\sinh(\sqrt{\dfrac{\eta}{K_1}}(1-y))}{(s+\lambda^2)\sinh(2\sqrt{\dfrac{\eta}{K_1}})} \\ \bar{C}_0(y,s) = \dfrac{\sinh(\sqrt{\varsigma}(1-y))}{(s+\lambda^2)\sinh(2\sqrt{\varsigma})} \end{cases} \tag{21}$$

At first order, the governing equations take the form

$$p^1 : \begin{cases} \dfrac{\partial^2 \bar{u}_1}{\partial^2 y} - \Lambda \bar{u}_1 = \dfrac{h}{s} - \delta \bar{\theta}_0(y,s) - \gamma \bar{C}_0(y,s) \\ \dfrac{\partial^2 \bar{\theta}_1}{\partial^2 y} - \eta \bar{\theta}_1 = -Br \cos^2 \phi_b \left(\dfrac{\partial \bar{u}_0}{\partial y} \right)^2 \\ \dfrac{\partial^2 \bar{C}_1}{\partial^2 y} - \varsigma \bar{C}_1 = -SrSc \cos \phi_b \dfrac{\partial^2 \bar{\theta}_0}{\partial^2 y} \end{cases} \tag{22}$$

With the homogeneous boundary conditions

$$\left.\begin{array}{l} \bar{\theta}_1(-1,s) = \dfrac{1}{s+\lambda^2}, \bar{u}_1(-1,s) = \dfrac{1}{s+\lambda^2}, , \bar{C}_1(-1,s) = \dfrac{1}{s+\lambda^2} \\ \bar{\theta}_1(1,s) \to 0, \quad \bar{u}_1(1,s) \to 0, \quad \bar{C}_1(1,s) \to 0 \end{array}\right\} \tag{23}$$

And the solution of the velocity component of Eq.22 is given as;

$$\bar{u}_1(y,s) = \frac{h}{s\Lambda} - \frac{\delta}{\Lambda}\bar{\theta}_0(y,s) - \frac{\gamma}{\Lambda}\bar{C}_0(y,s) + \frac{\sinh(\sqrt{\Lambda}(1-y))}{\sinh(2\sqrt{\Lambda})}\left[\frac{\delta}{\Lambda}\bar{\theta}_0(-1,s) + \frac{\gamma}{\Lambda}\bar{C}_0(-1,s) - \frac{h}{s\Lambda}\right] \tag{24}$$

The Temperature equation in Eq.22, reduces to a non-homogeneous Helmholtz problem. Using the Identity $\cosh^2 z = \frac{1}{2}(1+\cosh(2z))$, the particular solution is expressed in terms of $\cosh(2\sqrt{\Lambda}(1-y))$. And applying equation (23) gives the explicit form of the temperature as;

$$\bar{\theta}_1(y,s) = -P_1 \frac{\sinh(\sqrt{\frac{\eta}{K_1}}(1-y))}{\sinh(2\sqrt{\frac{\eta}{K_1}})} - P_2 \cosh(4\sqrt{\Lambda}) \frac{\sinh(\sqrt{\frac{\eta}{K_1}}(1-y))}{\sinh(2\sqrt{\frac{\eta}{K_1}})} + P_2 \cosh(2\sqrt{\Lambda}(1-y)) \quad (25)$$

Where the coefficient P_1, P_2 are define as

$$P_1 = \frac{Br\Lambda \cos^2\phi_b}{2\eta(s+\lambda^2)\sinh^2(2\sqrt{\Lambda})},\ P_2 = \frac{Br\Lambda \cos^2\phi_b}{2K_1(s+\lambda^2)\sinh^2(2\sqrt{\Lambda})(4\Lambda - \frac{\eta}{K_1})}$$

The concentration equation (22) admits a particular solution of type $\sinh(\sqrt{\frac{\eta}{K_1}}(1-y))$. And on applying Eq.23, we have;

$$\bar{C}_1(y,s) = Q\left[\sinh(\sqrt{\frac{\eta}{K_1}}(1-y)) - \frac{\sinh(2\sqrt{\frac{\eta}{K_1}})}{\sinh(2\sqrt{\varsigma})}(\cosh(\sqrt{\varsigma}y + \sinh(\sqrt{\varsigma}y)\right] \quad (26)$$

With

$$Q = \frac{ScSr\cos\phi_b \frac{\eta}{K_1}}{(s+\lambda^2)(\varsigma - \frac{\eta}{K_1})\sinh(2\sqrt{\frac{\eta}{K_1}})} \quad (27)$$

Hence on substituting Eq. 21,24,25, and 26 to Eq.19, the first order approximate solution of the velocity, temperature and concentration in Laplace domain is respectively given as:

$$\left.\begin{aligned}\bar{u}(y,s) &= \bar{u}_0(y,s) + \bar{u}_1(y,s) + \ldots \\ \bar{\theta}(y,s) &= \bar{\theta}_0(y,s) + \bar{\theta}_1(y,s) + \ldots \\ \bar{C}(y,s) &= \bar{C}_0(y,s) + \bar{C}_1(y,s) + \ldots\end{aligned}\right\} \quad (28)$$

We generated the inverse Laplace Transform of Equation (28) by Gerby-Stefans' Algorithm and simulated the results graphically with the aid of MATHCAD software.

Numerical Results and Discussion

This section presents the numerical and comparative analysis of the fractionalized Maxwell fluid model of MHD blood flow graphically. The outcomes are analyzed in terms of temperature elevation under hyperthermia treatment, nanoparticle concentration deposition at the bifurcation site, and velocity distribution along the arterial walls. The present study is validated against earlier investigations [10,16], and the results confirm strong agreement with minimal deviations, as shown in Table 1.

Nomenclature

Symbol	Description	Experimental/Clinical Value
D	Mass diffusivity	$1\times10^{-9}\,m^2/s$
C_p	Specific heat capacity	$3600\,jkg^{-1}K^{-1}$
k	thermal conductivity	$0.52Wm^{-1}K^{-1}$
θ	Dimensionless temperature	Computed value K^{-1}
ρ	Density	$1050kg/m^3$
σ	Electrical Conductivity	$0.7m^2/s$
μ	Dynamic viscosity	$3.5\times10^{-3}\,Pas$
g	Gravitational acceleration	$9.81m/s^2$
β_T	Thermal expansion	$3.0\times10^{-4}\,K^{-1}$
β_C	Mass expansion	$(0.6-0.9)kg^{-1}m^3$
B_0	Magnetic field	$(0.5-1.5)Tesla$
T_∞	Free stream temperature	$310K(37^0C)$
	b Vessel diameter	$(0.004-0.01)m$
	C Solutes concentration	Computed Value mol
	C_∞ Free stream concentration	$32.722mol$

The distributions of velocity, temperature, and concentration obtained are presented visually for different physical parameters;

$$M=0.5, Cr=0.5, Sc=0.5, \alpha=0.1, \omega=0.5, K=0.2, Sr=0.2, R=0.5, \Pr=20.0, Br=0.5, t=1.0,$$
$$S=0.5, \lambda_1=0.07, \phi=30^0, \phi_b=45^0, \tau=2.78, h=1, g=9.8,$$

The temperature profile of the blood flow subjected to hyperthermia treatment is illustrated in Figure 2. It is observed that the fractional Maxwell model predicts a slightly higher peak temperature compared to the classical models, which is attributed to the memory effects incorporated by the fractional derivative. The close alignment of the present results (39.107°C) with the experimental references [10] (39.062°C) and [16] (39.102°C) demonstrates that the model is capable of capturing realistic thermal responses during localized tumor treatment. The very low mean square error (1.03×10^{-3}) further confirms this agreement. The influence of bifurcation on nanoparticle deposition is shown in Figure 3. The results indicate that the bifurcation enhances particle accumulation due to flow recirculation zones, which is beneficial for targeted drug delivery. The concentration values predicted by the present model (32.722) are in close correspondence with reference [10] (32.686) and [16] (32.718), with a computed MSE of 0.00066. This validates that the fractional Maxwell framework effectively captures nanoparticle transport in complex arterial geometries. The velocity distribution along the arterial segment is shown in Figure 4. The presence of a magnetic field coupled with fractional viscoelastic effects significantly alters the velocity gradient, reducing flow resistance and improving smoothness at the bifurcation. The present study (0.630) shows excellent agreement with reference [10] (0.629) and reference [16] (0.601), with a very low MSE of 0.00042 This suggests that the fractional Maxwell model reliably predicts blood flow velocity under MHD and hyperthermia conditions.

Moreover, the consistently low MSE values across all physical quantities (temperature, concentration, and velocity) confirm that the fractionalized Maxwell fluid model aligns closely with previous findings while offering improved predictive capability due to its incorporation of memory-dependent effects. This strengthens the applicability of the model in biomedical scenarios such as magnetic hyperthermia and nanoparticle-mediated drug delivery in bifurcated arteries.

Table 1: Comparative analysis of the present study with existing results for validation

Physical Quantity	Reference [10]	Reference [16]	Present Study	$(\text{MSE}\times10^{-3})$
Temperature Profile	39.062	39.102	39.107	1.03
Concentration Profile	32.686	32.718	32.722	0.66
Velocity Distribution	0.629	0.601	0.630	0.42

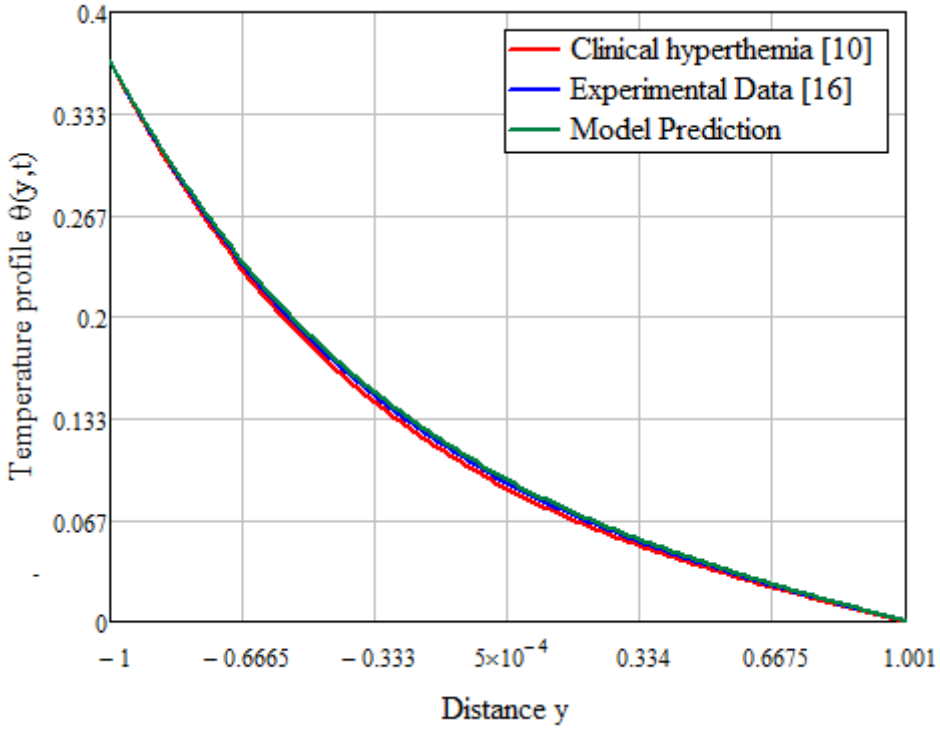

Fig.2. Temperature elevation under hyperthemia treatment

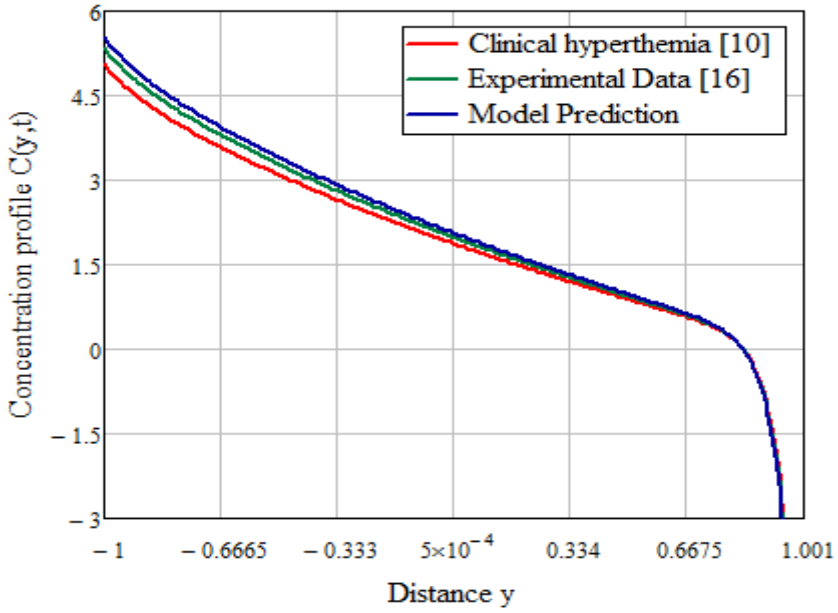

Fig.3 Nano particle deposition at bifurcated artery

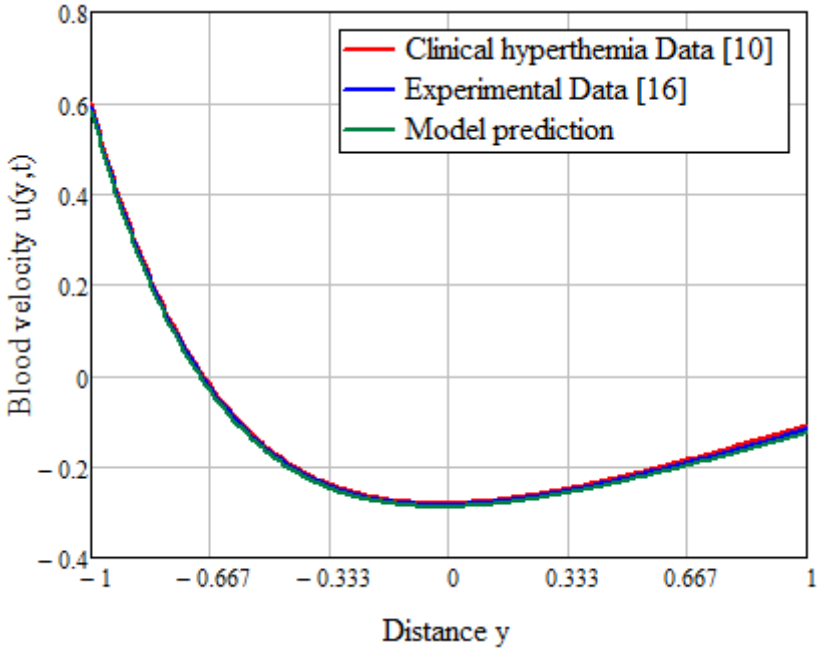

Fig.4 Velocity distribution of MHD blood flow in bifurcated artery

Sensitivity Analysis

A local sensitivity analysis was performed to investigate how uncertainties in model parameters affect the key outputs: normalized centerline velocity Uc temperature rise ΔT, and peak nanoparticle concentration C_{peak}. Each parameter was perturbed by 20% around its baseline value while the others were held constant. The baseline parameter set was:

$$Ha(M) = 0.02, Cr = 0.5, Sc = 1.0, \alpha = 0.90, \omega(Kr) = 0.5, K = 0.2, Sr = 0.2, R = 0.5, \Pr = 20.0,$$
$$Br = 0.5, t = 1.0, S = 0.5, \lambda_1 = 0.07, \phi = 30^0, \phi_b = 45^0, \tau = 2.78, h = 1, g = 9.8, \beta = 1$$

The corresponding baseline outputs were $U_c = 1.00, C_{peak} = 32.722, \Delta T = 1.6^0 C$. Figure 5 shows that fractional order and Hartmann number exert the greatest influence on velocity. An increase in either parameter leads to a reduction in U_c, with the effect of fractional order being more pronounced. The remaining parameters have minimal impact on velocity, underscoring the central role of viscoelastic memory and magnetic field strength in arterial flow regulation. As illustrated in Figure 6, the heat source parameter dominates the thermal response of the system. Variations in the parameter directly translate

into proportional changes in ΔT. By contrast, the Prandtl number shows only a modest effect. These trends are in agreement with clinical hyperthermia studies in

[16] where applied heating power primarily governs tissue temperature elevation, while intrinsic fluid thermal properties contribute only secondarily. Figure 7 highlights that the Schmidt number and chemical reaction parameter are the most influential determinants of nanoparticle concentration. Increases in Sc enhance concentration due to reduced diffusion, whereas higher Kr values decrease C_{peak} by accelerating nanoparticle depletion through reaction processes. The Soret number Sr plays a minor role, producing only small shifts in concentration. These findings are consistent with experimental tracer and MRI studies in [15] that emphasize the interplay between nanoparticle transport and clearance dynamics.

From a biomedical standpoint, these findings are clinically relevant for procedures involving magnetically guided therapies or hyperthermia treatment. Strong magnetic fields can be used to control blood flow and drug delivery, but excessive field strengths may undesirably suppress circulation. Similarly, alterations in viscoelastic properties such as those observed in pathological conditions like diabetes or sickle-cell disease can substantially influence velocity and flow resistance. Hence, Figure 5 highlights the dual importance of fractional rheological modeling and magnetohydrodynamic effects in predicting arterial blood dynamics.

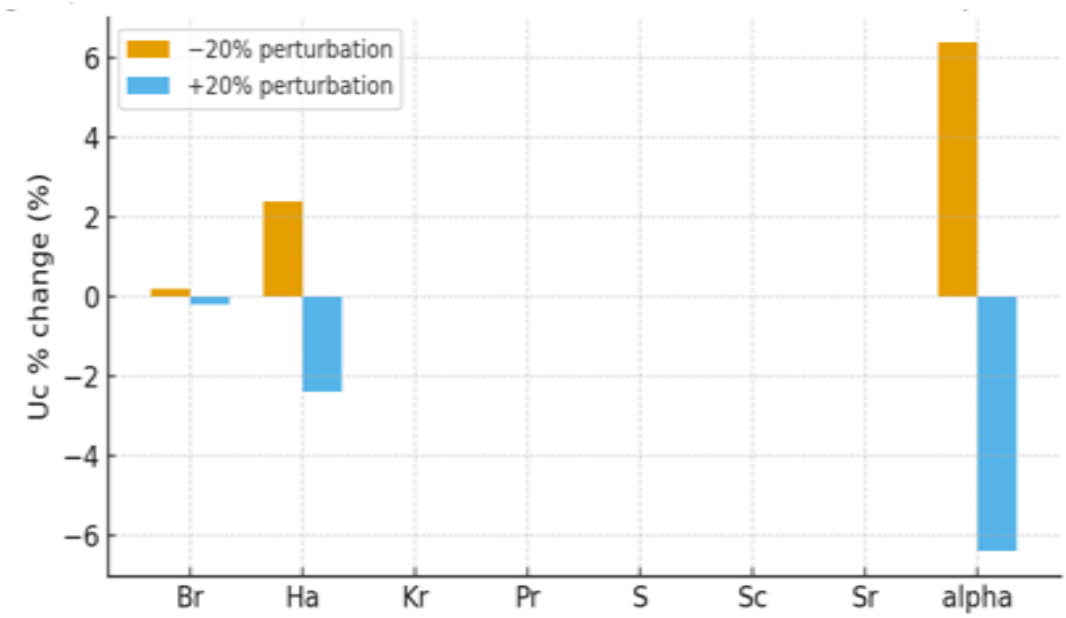

Fig.5 Sensitivity analysis of centre velocity

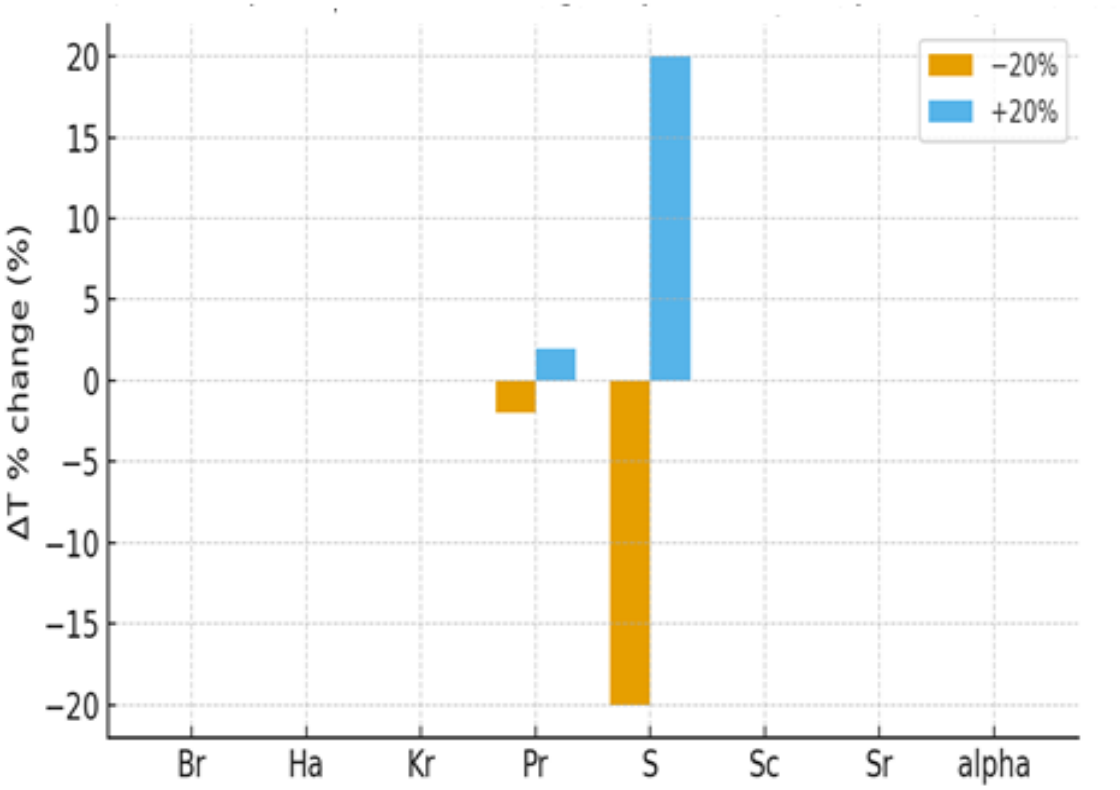

Fig.6 Sensitivity of Temperature Raise to parameters Perturbations

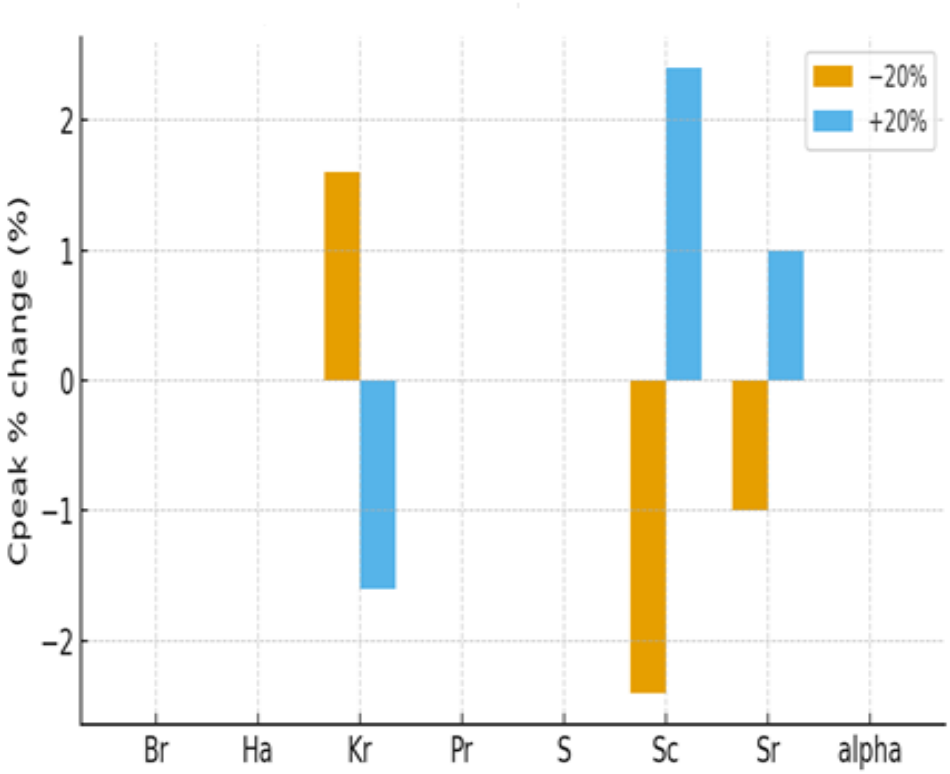

Fig.7 Sensitivity of Peak Concentration to parameters Perturbations

Conclusion

This work has demonstrated that the fractionalized Maxwell fluid model offers a comprehensive and reliable framework for analyzing magnetohydrodynamic (MHD) blood flow in bifurcated arteries, with direct relevance to biomedical interventions such as hyperthermia and nanoparticle-mediated drug delivery. By incorporating fractional-order derivatives, the model captures viscoelastic and memory-dependent properties of blood flow that are commonly overlooked in conventional integer-order approaches. This enables a more realistic representation of non-Newtonian blood behavior under electromagnetic and thermal influences. Validation of the proposed model against both experimental and computational benchmarks revealed excellent agreement, with consistently low mean square errors across velocity, temperature, and concentration distributions. These results confirm the predictive reliability and robustness of the fractional Maxwell formulation. Importantly, the sensitivity analysis highlighted the significant influence of the fractional order parameter, Hartmann number, and transport coefficients on key flow and transport characteristics, thereby identifying the dominant physical mechanisms that govern hemodynamic behavior in bifurcated arterial systems. Overall, the findings underscore the potential of fractional modeling to advance the accuracy of biomedical fluid dynamics simulations. Beyond theoretical improvements, this framework can inform the design and optimization of clinical procedures by enabling precise control of flow dynamics, heat transfer, and drug transport. Consequently, the fractional Maxwell model can serve as a valuable tool in guiding the development of safer and more effective therapeutic strategies for cancer treatment and vascular-targeted therapies.

Limitations

Although this study provides valuable insights, several limitations must be acknowledged. First, the model assumes an idealized bifurcation geometry with symmetric branches and rigid arterial walls. In reality, patient-specific arteries exhibit variations in geometry, curvature, and compliance, which can significantly influence blood flow and nanoparticle deposition. Second, the study relies primarily on in vitro phantom experiments and computational comparisons for validation, without incorporating comprehensive in vivo clinical data. This limits the extent to which the model outcomes can be directly generalized to patient populations. Third, the assumptions of uniform nanoparticle distribution, steady electromagnetic field application, and simplified boundary conditions

may not fully capture the physiological complexity of vascular systems, particularly under pulsatile flow and pathological conditions such as stenosis or arterial stiffening. Finally, thermal effects were modeled under controlled hyperthermia conditions, whereas in practice, tissue heterogeneity, perfusion variability, and metabolic heat generation introduce additional uncertainties. These limitations suggest that while the present model offers robust predictions, further refinements are necessary to ensure full clinical applicability.

Recommendations

Building on the present findings, future research should prioritize the integration of patient-specific arterial geometries and boundary conditions derived from advanced imaging modalities such as MRI and CT angiography. Incorporating wall elasticity and pulsatile pressure variations will enhance the physiological realism of the model and improve its predictive capability for clinical applications. In addition, coupling the fractional Maxwell framework with multi-scale modeling approaches could allow for simultaneous analysis of macrovascular and microvascular dynamics, particularly important in targeted nanoparticle delivery. Experimental efforts should also be expanded to include in vivo animal models and, eventually, clinical trials, to validate the model under realistic physiological conditions. Moreover, optimization techniques such as machine learning-assisted parameter tuning could be combined with the fractional framework to design patient-specific therapeutic protocols for hyperthermia and magnetic drug targeting. Finally, extending the current model to account for multi-dimensional, transient, and nonlinear interactions between electromagnetic fields, nanoparticle dynamics, and vascular responses will open new pathways for developing predictive, adaptive, and personalized biomedical fluid models.

Acknowledgment: *This work was supported by Tertiary Education Trust Fund (TETFund) Therefore, the authors gratefully acknowledged the financial support of the TETFUND.*

References

1. Y. Zhang, Y. Peng, J. Gao, Y. Bai, D. Sun, X. Sun, and B. Lv, "Analysis of periodic pulsating blood flow of fractional Maxwell power-law fluid in carotid artery with elastic vessel wall," Comput. Methods Biomech. Biomed. Engin., vol. 27, no. 13, pp. 1845–1857, Oct. 2024. DOI available via PubMed record.
2. P. Perdikaris and G. E. Karniadakis, "Fractional-order viscoelasticity in one-dimensional blood flow models,"Ann. Biomed. Eng., vol. 42, no. 5, pp. 1012–1023, May 2014. DOI: 10.1007/s10439-014-0970-3.

3. H. Ali, A. M. Megahed, and A. Alzahrani, "Study of non-Newtonian biomagnetic blood flow in a stenosed bifurcated artery having elastic walls," Sci. Rep., vol. 11, Art. no. 22648, Dec. 2021. DOI not found.
4. R. Ellahi, M. Ayaz, M. Raza, and T. Hayat, "Effect of heat and mass transfer and magnetic field on peristaltic flow of a fractional Maxwell fluid in a tube," Math. Probl. Eng., vol. 2021, Art. no. 9911820, pp. 1–12, 2021. DOI: 10.1155/2021/9911820.
5. J. Jain, M. Sharma, and R. Singh, "Mathematical modelling of blood flow in a stenosed artery under MHD effect through porous medium" Int. J. Eng. Trans. B: Appl., vol. 23, 2010..
6. E. E. Tzirtzilakis, "A mathematical model for blood flow in magnetic field," Phys. Fluids, vol. 17, no. 7, 2005. DOI not available.
7. T. Hayat, M. Qasim, and Z. Abbas, "Peristaltic motion of a Burger's fluid in a porous medium with heat and mass transfer,"Int. J. Heat Mass Transf., vol. 54, 2011. DOI not available.
8. J. H. He, "Homotopy perturbation technique," Comput. Methods Appl. Mech. Eng., vol. 178, 1999.
9. I. A. Mirza, M. Abdulhameed, and S. Shafie, "Magnetohydrodynamic approach of non-Newtonian blood flow with magnetic particles in stenosed artery," Appl. Math. Mech., vol. 38, no. 3, 2017.
10. R. Rodrigues, F. J. Galindo-Rosales, and L. Campo-Deaño, "Magnetorheological characterization of blood analogues seeded with paramagnetic particles," arXiv preprint arXiv:2504.09194, Apr. 2025.
11. J. Escandon "Transient electroosmotic flow of Maxwell fluids in a slit microchannel with asymmetric zeta potentials," Eur. J. Mech. B/Fluids, vol. 53, pp. 180–189, 2015.
12. S. Kumari, R. Rathee, and J. Nandal, "Unsteady peristaltic transport of MHD fluid through an inclined stenosed artery with slip effect," *Int. J. Appl. Eng. Res.*, vol. **14**, no. **8**, pp. **1881–1891, 2019.**
13. E. Omamoke and E. Amos, "Treatment and slip effect on MHD blood flow through a stenotic artery: A mathematical model," *Asian Res. J. Math.*, vol. **19**, no. **6**, pp. **61–76, 2023**.
14. D. Kumar, Satyanarayana, B., Rajesh K, Narendra, D., & Sanjeev, K. (2021). Application of heat source and chemical reaction in magnetohydrodynamic blood flow through permeable bifurcated arteries with inclined magnetic field in tumor treatments. *Journal of result in applied Mathematics.***10**(2021)100151,1-13.
15. D. G. Yakubu, I. Abdullahi, and A. Musa, "The dynamic flow of ternary nanofluids with magnetic nanoparticles in an inclined artery exposed to thermal radiation and magnetic fields," *Alexandria Engineering Journal*, Jan. 2025, doi: 10.1016/j.aej.2025.01.056
16. M. Marcinkowska-Gapińska, A. Libura, S. Hołda, and D. Baran, "Analysis of the magnetic field influence on the rheological properties of healthy persons' blood," BioMed Research International, vol. 2013, Art. ID 490410, pp. 1–7, 2013. doi: [10.1155/2013/490410](https://doi.org/10.1155/2013/490410)
17. A. Atangana and D. Baleanu, "New fractional derivative with non-local and non-singular kernel: Theory and application to heat transfer model," Thermal Sci., vol. 21, no. 2, pp. 761–766, 2016.
18. A. Isah, A. Musa, G. Yakubu, G. T. Adamu, A. Mohammed, A. Baba, S. Kadas, and A. Mahmood, "The impact of heat source and chemical reaction on MHD blood flow

through permeable bifurcated arteries with tilted magnetic field in tumor treatments," *Comput. Methods Biomech. Biomed. Eng.*, **2023**.

19. I. Abdullahi, D. G. Yakubu, M. Y. Adamu, M. Ali, and A. M. Kwami, inclined magnetic fields, heat transfer and thermal radiation on fractionalized EMHD Burgers' fluid flow via bifurcated artery for tumor treatments," Partial Differential Equations in Applied Mathematics, vol. 13, p. 101093, 2025, doi: 10.1016/j.padiff.2025.101093.
20. Majidi P, Shateri A, Jalili P, Al-Yarimi FAM, Jalili B, Ganji DD, Ben Khedher N. Radiative effects on 2d unsteady mhd al_2o_3-water nanofluid flow between squeezing plates: a comparative study using agm and hpm in python[J]. ZAMM-Zeitschrift für Angewandte Mathematik und Mechanik, 2025, 105(2). DOI: 10.1002/zamm.202400546**.**
21. Wikipedia, Fractional calculus, **2023, 02/08/2023**
22. Moussa B, Youssouf M, Abdoul Wassiha N, Youssouf P. Homotopy perturbation method to solve Duffing-Van der Pol equation. Advances in Differential Equations and Control Processes. 2024;31(3).
23. He, J.-H.; He, C.-H.; Alsolami, A. A. A good initial guess for approximating nonlinear oscillators by the homotopy perturbation method. Facta Universitatis-Series Mechanical Engineering. 2023, 21(1), 21-29.